ACS APPLIED MATERIALS & INTERFACES

RESEARCH ARTICLE

www.acsami.org

Chemical Tailoring of Hybrid Sol−Gel Thick Coatings As Hosting Matrix for Functional Patterned Microstructures

Paolo Falcaro,*[,†] Stefano Costacurta,[‡] Luca Malfatti,[§] Dario Buso,[†,⊥] Alessandro Patelli,[‡] Piero Schiavuta,[‡] Massimo Piccinini,[#] Gianluca Grenci,[||] Benedetta Marmiroli,[¶] Heinz Amenitsch,[¶] and Plinio Innocenzi*[,§]

[†]Division of Materials Science and Engineering, CSIRO, Private Bag 33, Clayton South MDC, Victoria 3169, Australia

[‡]Associazione CIVEN−Nano Fabrication Facility, Via delle Industrie 9, 30175 Venezia, Italy

[§]Laboratorio di Scienza dei Materiali e Nanotecnologie (LMNT), CR-INSTM, Università di Sassari, Palazzo Pou Salid Piazza Duomo 6, 07041 Alghero SS, Italy

[⊥]Centre for Micro-Photonics and CUDOS, Faculty of Engineering and Industrial Sciences, Swinburne University of Technology, Hawthorn, Victoria 3122, Australia

[#]Porto Conte Ricerche s.r.l., S.P. 55, km 8,400, 07041 Alghero SS, Italy

[||]CNR-IOM, Laboratorio TASC, S.S. 14, Km 163.5 in Area Science Park, 34012 Basovizza, Trieste, Italy

[¶]Institute of Biophysics and Nanosystems Research, Austrian Academy of Sciences, Schmiedlstrasse 6, 8042 Graz, Austria

Supporting Information

ABSTRACT: A phenyl-based hybrid organic − inorganic coating has been synthesized and processed by hard X-ray lithography. The overall lithography process is performed in a two-step process only (X-rays exposure and chemical etching). The patterns present high aspect ratio, sharp edges, and high homogeneity. The coating has been doped with a variety of polycyclic aromatic hydrocarbon functional molecules, such as anthracene, pentacene, and fullerene. For the first time, hard X-rays have been combined with thick hybrid functional coatings, using the sol−gel thick film directly as resist. A new technique based on a new material combined with hard X-rays is now available to fabricate optical devices. The effect due to the high-energy photon exposure has been investigated using FT-IR and Raman spectroscopy, laser scanner, optical profilometer, and confocal and electron microscope. High-quality thick hybrid fullerene-doped microstructures have been fabricated.

KEYWORDS: sol−gel films, hybrid materials, lithography, fullerenes, acene

INTRODUCTION

Patterning technology allows for writing materials in controlled spaces and it represents a fundamental step toward device fabrication. An open challenge in recent research is to find easier, faster, and more versatile lithographic protocols.[1]

UV and X-ray lithographic processes are common patterning technologies available for device fabrication. Beside soft-lithographic methods,[2] an alternative is the deep X-ray lithography (DXRL), which employs high energy photons and has some unique properties and advantages if combined with sol−gel processing.[3] Intense X-ray radiation can be used to break the organic bonds and induce condensation of the inorganic network in controlled areas of the sample. These two effects have been recently investigated using infrared spectroscopy[4] and different types of silica based coatings have been patterned using hard X-rays. The combination of sol−gel with X-rays allows for one-step lithography of functional coatings; the same wavelengths have been exploited to pattern mesoporous silica, organic−inorganic hybrid mesoporous coatings, and hierarchical porous films.[5,6] Furthermore, the high-energy photons have been used to induce simultaneous metallic nanoparticles formation and growth,[7] decomposing the organic templates in mesostructured silica films,[6] or damaging the dye molecules grafted on the surface or embedded in SiO_2 hybrid coatings.[1,3] DXRL has been also efficiently applied to pattern hybrid organic−inorganic thick films prepared via plasma-enhanced chemical vapor deposition (PE-CVD).[8] These examples demonstrate the possibility to pattern functional coatings of different thickness with no need for additional resists or photoactivators. In comparison with the majority of conventional lithographic microfabrication techniques, which require a three-step process, DXRL is attractive because it allows for a simpler one- or two-step lithography. In fact, under the proper conditions, the functional material can be directly used as a resist. The drawback is clearly the need of an intense source of X-rays, such as a synchrotron light, which limits the diffusion of the technology. An advantage of DXRL process is the high penetration depth of the high-energy photons and therefore DXRL is normally used to pattern thick polymer resist layers.[9] With a proper choice of the materials, the irradiation conditions, and the etching protocols, high-aspect-ratio structures and submicrometer resolution can be obtained.[10,11] Spatial resolutions below 10 nm have been obtained using X-rays,

Received: September 21, 2010
Accepted: December 13, 2010
Published: January 10, 2011

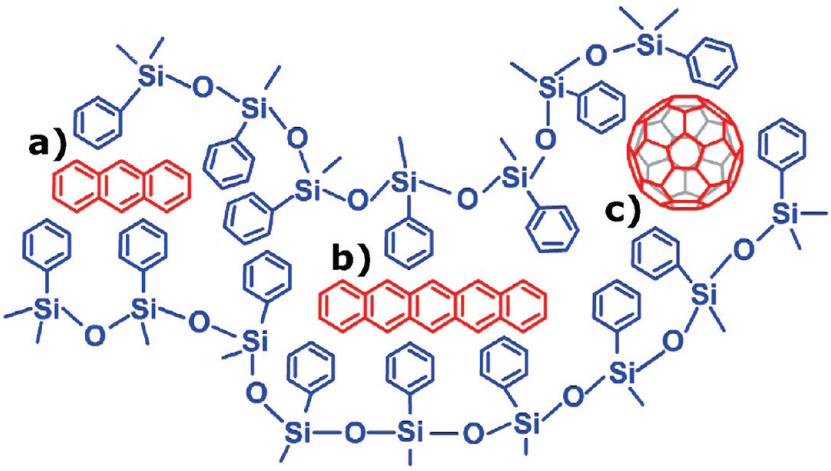

Figure 1. Schematic of the doped phenylsilane coating with (a) anthracene, (b) pentacene, and (c) fullerene. The phenyl groups allow for the homogeneous dispersion of functional polycyclic aromatic molecules.

therefore knowledge related to X-ray lithography is fundamental for the nanofabrication of new devices, especially for optical applications. Despite the huge number of studies investigating polymeric resists and hard X-rays, only few works reporting patterning on thick hybrid organic−inorganic resists can be found;[12,13] however, even if the patterns are proposed for micro-optical applications, better protocols are needed to achieve sufficient device quality. In fact, patterns with imprecise edges and a moderate aspect ratio have been obtained. In the present study, customized recipes and protocols are presented in order to obtain high-quality phenyl-silane patterns. In the literature, phenylsilane coatings are presented as relevant technological materials for fabrication processes in electronics, optics, and sensing.[14,15] Usually, chemical modification of the phenyl termination (e.g., tert-butyl groups) or additional external photosensitizers (e.g., 3,3′,4,4′-tetra (t-butylperoxycarbonyl)-benzophenone) are needed if UV light is used to irradiate the sample.[14] In the present study, using hard X-ray lithography, chemical modifications or external additive are not needed anymore and the functional material can be used directly as a resist. In fact, high-aspect-ratio patterns have been obtained in the 1−100 μm thickness range. The proposed sol gel resist presents also further appealing features for the fabrication of customized optical devices. In fact, as presented in Figure 1, functional organic compounds that usually cannot be introduced into conventional low-melting glasses can be embedded into phenyl modified polysiloxane glasses due to the high affinity for the phenyl group bonded to the siloxane network.[16] Therefore important functional polycyclic aromatic molecules for optical applications (anthracene,[17] pentacene,[18] and fullerene[19,20]) can now be homogeneously dispersed and patterned for the fabrication of new devices.

EXPERIMENTAL SECTION

Film Preparation. Phenyltriethoxysilane (PhTES), anthracene, pentacene, fullerenes (C_{60}, 98%), hydrochloric acid 1M, isopropanol, and toluene were purchased from Aldrich and used as received; p-type boron-doped silicon wafers were employed as the substrates.

The precursor sol for the deposition of bare hybrid thick films was prepared adding 6 mL of PhTES into a mixture of 12 mL of toluene and 6 mL of isopropanol. After stirring for 10 min at reflux temperature (about 72 °C), 1.5 mL of HCl 1 M was added dropwise: the solution turned opaque immediately after the addition of HCl and then became transparent in few seconds. The sol was kept under stirring for 4.5 h in a 250 mm long neck open flask under reflux conditions. At this stage, the hydrolyzed sol is ready to be either deposited on silicon wafers or doped with the polycyclic aromatic hydrocarbon based functional molecules. Thick films (1−5 μm) were prepared by spin-coating (2000−500 rpm), whereas films with thicknesses up to 100 μm were obtained via casting.

To prepare the C_{60} doped phenylsilane coating, we dispersed 2.5 mg of C_{60} in 2 cc of toluene; after complete solubilization under sonication, the solution appeared violet and transparent. The C_{60} solution was then added to the hydrolyzed sol and stirred for 10 min. Similarly, acene-doped phenylsilane coatings were prepared adding 10−60 mg of anthracene or pentacene to the precursor sol; the films were prepared by casting the sol on a silicon wafer. The coatings were dried for 2 h in air at 30% RH and then prebaked for 2 h at 60 °C. The emission spectra of the anthracene doped sol−gel coating matches that of anthracene dispersed in toluene (see the Supporting Information), proving that anthracene molecules are efficiently solvated by phenyl groups in the hybrid film. Both Raman fluorescence and linear absorption spectra measured on the PhTES-C_{60} hybrid coating evidence the presence of isolated C_{60} molecules, or clusters with a number of molecules lower than 10 (see the Supporting Information); this demonstrates that the fullerene has been efficiently solvated by phenyl groups as well.

Patterning Process. The films were directly exposed to hard X-rays using the Deep X-ray Lithography beamline (DXRL) at Elettra synchrotron facility (Trieste, Italy). The films were irradiated with different doses by changing the exposure time (12.5, 25, 50, 100, 200, and 400 s). The films were exposed to energies per unit area incident to the sample surface corresponding to 94, 188, 377, 754, 1508, and 3015 $J \cdot cm^{-2}$. Note that the energy per unit area is equal to the exposure time multiplied by a factor 7.53 which is a power per unit area incident on the sample surface. The sample was mounted on the top of a water cooled stainless steel plate (scanner), which was continuously rastering the sample to obtain a homogeneous exposure of areas larger than the beam size, the scanner rate was set to 20 mm s^{-1}. At the exposure plane (position of the sample) the beam size was 115.5 × 10.6 mm^2.

After exposing to X-ray radiation, the sample was dipped in propylene glycol methyl ether acetate (PGMEA), commercially known as SU-8 resist developer, for a time related to the thickness of the irradiated film (typically 20 s are enough to develop a 30 μm thick film). Rinsing was done in isopropyl alcohol for 15 s, and finally, the sample was dried with flowing nitrogen to avoid remaining residuals.

Materials Characterization. Fourier transform infrared (FTIR) measurements were performed using a Vertex 70 Bruker spectrometer in

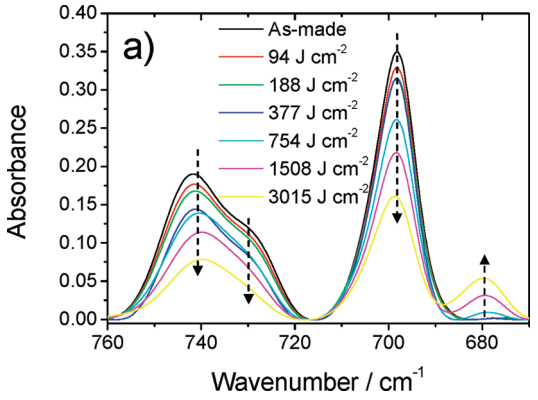

Figure 2. FTIR absorption spectra, in the 760 −670 cm^{-1} range, of phenylsilane films exposed to different X-ray doses. The arrows show the directions of intensity changes increasing the dose.

the 375−4000 cm^{-1} range with a resolution of 4 cm^{-1}; a RT-DTGS detector and a KBr beam splitter were used. The baseline was corrected by a concave rubberband method (OPUS 6.5 software) using 64 baseline points and 4 iterations.

A Bruker Senterra confocal Raman microscope working with a laser excitation wavelength of 785 nm at 100 mW of nominal power was used for Raman imaging. A 20× objective was selected and an array of 52 × 52 points was defined to cover an area of 72.8 × 72.8 μm^2 with a step of 1.4 μm. Each spectrum of the map was obtained by averaging 5 acquisitions of 4 s.

Sample surface images were observed by an optical microscope Nikon Optiphot 500.

A white-light optical profiler (ADE-Shift MicroXAM) was employed for 3D mapping of different patterned zones. The vertical excursion (z) was set between 5 and 50 μm as a function of the patterned film thickness; the recorded images were obtained with an average of 128 shots. Scanning Probe Image Processor (SPIP) software (Image Metrology, Hørsholm, Denmark) was used for image analysis.[21]

Scanning electron microscopy (SEM) was performed with a Zeiss Supra 40 instrument (Carl Zeiss MicroImaging GmbH, Germany).

RESULTS AND DISCUSSIONS

We have prepared hybrid coatings using phenyltriethoxysilane, as the organically modified alkoxide; these hybrid films are also an efficient host for a variety of polycyclic aromatic hydrocarbon-based functional molecules such as anthracene, pentacene, or fullerenes. In fact, functional organic compounds that usually cannot be introduced into conventional low-melting glasses can be introduced into phenyl modified polysiloxane glasses because of the high affinity for the phenyl group bonded to the siloxane network.[16] In this way, a chemical modification of fullerene is not needed to use its functional properties.[22] The hybrid films after processing are transparent and crack-free.

Effect of X-rays on Hybrid Materials. We have evaluated the effect of X-ray exposure on the hybrid materials by FTIR spectroscopy; we have performed a dose-matrix study, which consists of exposing a 1 μm thick coating deposited on a silicon wafer to increasing doses of X-rays and evaluating the effect by FTIR. The X-rays should produce degradation of organic bonds while at the same time promoting the densification of the inorganic network via reaction of the Si−OH species; these reactions are activated by the formation of free radicals by X-rays.[23]

Figure 2a shows the FTIR absorption spectra in the 760−670 cm^{-1} interval of the hybrid films exposed to increasing X-ray doses. Two main bands peaking around 740 and 700 cm^{-1}, which are attributed to vibrational modes of substituted benzene[24] and CH ring bending,[25] respectively, are observed; these bands show a similar trend and they decrease in intensity with the increase of the dose. The arrows in Figure 2 indicate the direction of change with increasing doses. Another band around 730 cm^{-1}, due to aromatic deformation, is overlapped to the 740 cm^{-1} signal and exhibits the same trend; it decreases in intensity with the dose. At lower wavenumbers, at 680 cm^{-1}, a band of smaller intensity is detected, but in this case, we observe a reverse response to X-ray exposure because the signal increases with increasing dose. The main effect that is induced by exposure of the film to intense X-rays is degradation of the phenyl rings; on the other hand some byproduct might also form, as indicated by the appearance of the new signal at 680 cm^{-1}. We assign this new band to wagging of C−OH groups which are formed as a consequence of X-ray exposure. Figure 3a shows the absorption FTIR spectra in the 1225−975 cm^{-1} range, which includes the Si−O−Si stretching

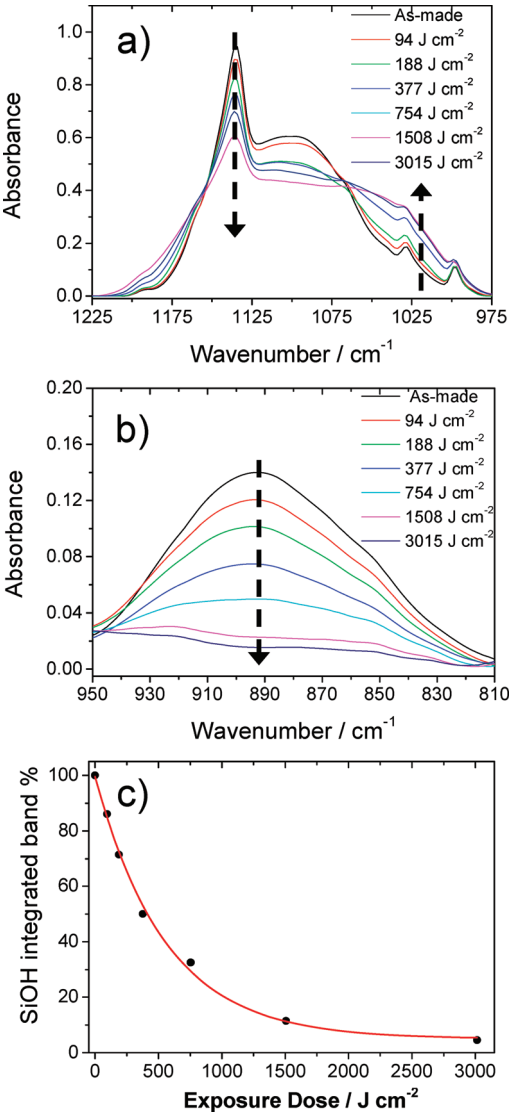

Figure 3. FTIR absorption spectra, in the (a) 1225−975 and (b) 950−810 cm^{-1} range, of phenylsilane films exposed to increasing X-ray doses. (c) Exponential decay of the integrated area relative to Si−OH band (950−810 cm^{-1}) as a function of X-ray dose.

region. The spectra appear composed of several overlapped bands; the bands at 1135, 1029, and 998 cm^{-1} are assigned to mono-substituted benzene ring modes.[26] The decrease in intensity of these bands at higher doses is similar to what we have observed in the spectra in Figure 2. The broad band peaking around 1080 cm^{-1} is, instead, assigned to Si−O−Si antisymmetric stretching and the band at around 900 cm^{-1} to Si−OH stretching (Figure 3b).[27] The presence of the silanol band indicates that the as deposited sample is not completely condensed and that the effect of X-rays is to induce a densification via condensation of Si−OH groups because the band decreases in intensity and finally disappears with the increase of the dose. Another band, which appears as an overlapped band around 1066 cm^{-1}, is observed. Attribution of this signal is not straightforward because several bands fall around this wavenumber. We think that this bands is also due to the formation of a by-product of the X-rays degradation of the organic side of the hybrid network. Following the literature, the band could be assigned to Si−O−C, C−O−C, or C−OH stretching[28]. Between these different possibilities, we have done the attribution looking at the FTIR spectra in the full range (4000−400 cm^{-1}) and searching for other vibrational modes that show a similar trend, i.e., they decrease with the increase of X-ray dose. We have found two bands that have this trend, at 680 and at 1480 cm^{-1}, which are assigned to the C−OH wagging and to the C−OH in-plane bending modes respectively; on the ground of this observation we have attributed the band at 1060 cm^{-1} to C−OH stretching. The effect of X-rays on the hybrid material can be summarized as follows: increasing doses of X-rays produce densification of the silica through condensation of Si−OH bonds, at the same time the X-rays induce degradation of organic bonds in phenyl rings and formation of C−OH species.

Integrating the FTIR spectra in the 950−810 cm^{-1} range we have calculated the change of the Si−OH band as a function of the dose. The results are shown in Figure 3c, the percentage variation has been calculated referring to the initial amount of Si−OH of the coating before irradiation. A first order exponential decay curve $y = 5.02 + 94.58e^{-(x/556)}$ fits properly the plotted data, with a calculated coefficient of determination (R^2) of 0.9972. All the doses are affecting the material and different quality patterns have been obtained increasing the exposure time; low exposure doses (94 and 188 J cm^{-2}) are not enough to ensure a good contrast between irradiated and unirradiated regions after the etching process. To give a reasonable contrast, we discovered that a minimum dose of 377 J cm^{-2} is needed; from our FTIR analysis, this provokes condensation of around 50% of the initial Si−OH.

DXRL on Hybrid Films. Immediately after deposition the hybrid films have been exposed to X-rays for writing different types of test patterns. Figure 4a presents an optical profilometry image of a 20 μm coating which has been patterned using a 377 J cm^{-2} exposure dose (50 s of exposure time). Defined the aspect ratio (AR) as the ratio of the height to the width of a patterned feature, the present pillar exhibits AR = 0.5 (see Figure 4b, height = H and width = BS, AR = H/BS). It is clearly visible that the structure could be even better defined; in fact, as shown in the Figure 4b, the ratio between the top section (TS) and base section (BS) of the pillar is about 0.8 and low frequency roughness induced by the lithography process is around 3 μm (a 15% of the pillar height, H).

A further increase in the energy to 754 J cm^{-2} allows for good-quality developed patterns as shown in Figure 5. This irradiation energy (corresponding to a condensation of around 68% of the initial silanols) is enough to simultaneously give a complete etching process of the exposed regions, while maintaining a flat surface of the structures for thicknesses in the 1−100 μm range (Figure 5). The percentage roughness is reduced to 2%; the best AR found is around 20 and the ratio TS/BS is 0.95. "Rings" of residuals are visible around the highest pillars, probably due to the rinsing process as shown by SEM images (Figure 5d). This has been observed only for high aspect ratio patterns when no flux of nitrogen gas has been used to remove the excess of isopropyl alcohol, in order to avoid any damage to the high aspect ratio pattern. After optimization of the rinsing process (i.e., rinsing the same pattern in different vessels of fresh isopropanol) the pattern appears without residuals. For all the other thinner patterned coatings, nitrogen gas can be used to remove residuals provoking no damage to the pattern. Figure 6 shows the 100 μm thick patterned and etched coating. The dark color represents the patterned phenylsilane coating, whereas the bright regions are the substrate (silicon). The same transparent color in the final pattern shows that the homogeneity is maintained along the whole lithographic process. From the optical image, no residuals can be detected in the etched regions, which confirms that the amount of residuals in the etched regions is very low.

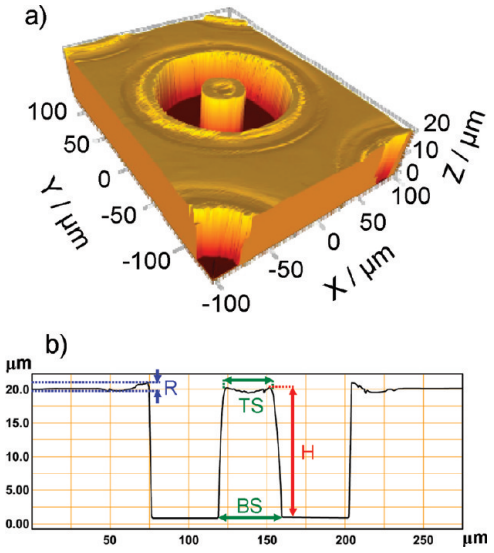

Figure 4. (a) 3D optical profilometry image of a 20 μm coating exposed to a 377 J cm^{-2} dose. (b) 2D depth profile of the same patterned microstructure. The plot has been obtained by scanning along a direction through the center of the pillar.

X-ray Lithography on Hybrid Functional Coatings. We have used Raman spectroscopy to characterize the hybrid functional materials upon exposure to X-rays. Figure 7 shows the Raman spectra in the 1440−1370 cm^{-1} interval of a hybrid film doped with anthracene, a spectrum of pure anthracene is reported as reference. In the unexposed (as made) anthracene-phenylsilane coating an intense band at 1402 cm^{-1} is detected (Figure 7a, black line) which is also found in the pure anthracene powder. It is the most intense one of such molecule and it is uniquely assignable to the $6A_g$ mode of anthracene.[29,30] After the exposure to hard X-ray, the A_g band disappears (Figure 7a, red line). Figure 7b shows an irradiated coating that did not undergo any chemical development process; the hexagonal perimeter represents the interface between the irradiated region (inside) and the unirradiated region (outside). Figure 7c has been generated, performing a Raman mapping in such an area and integrating the $6A_g$ mode in the 1420−1380 cm^{-1}

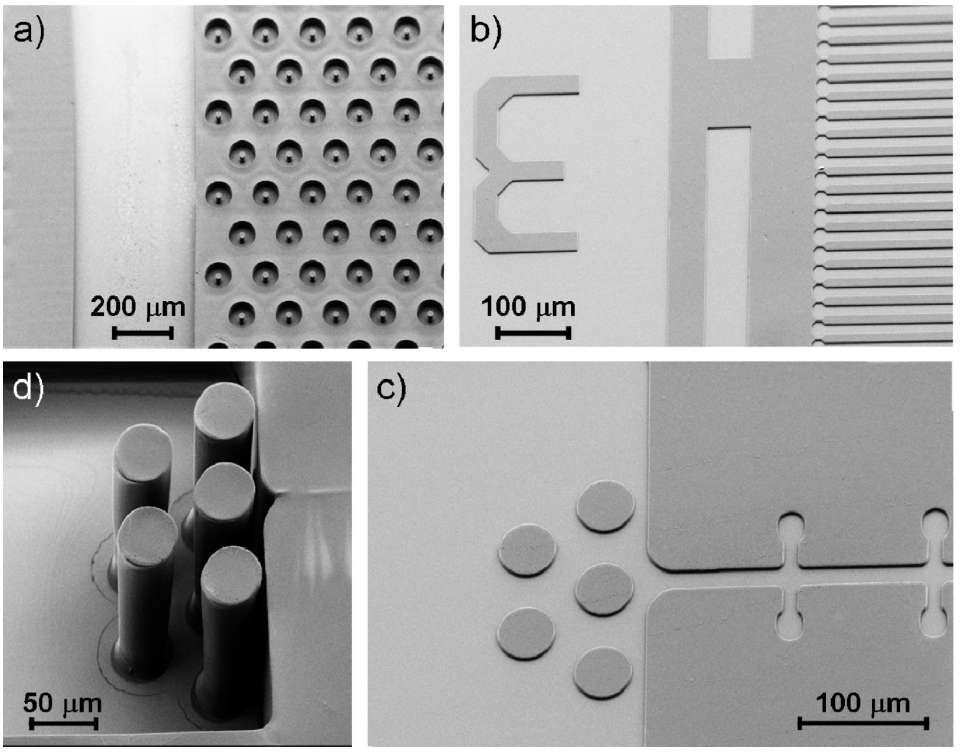

Figure 5. SEM images of hybrid organic−inorganic coatings with different thicknesses in the 1−100 μm range after exposing to 754 J cm^{-2} dose and rinsing with isopropanol.

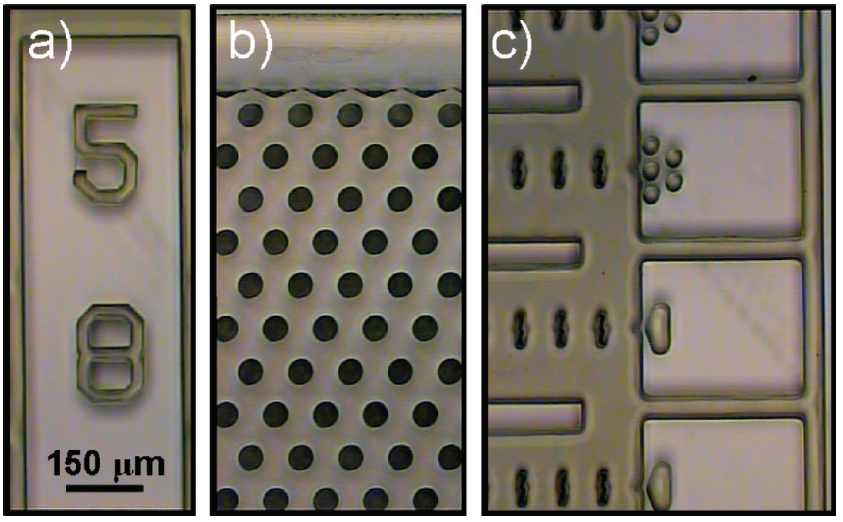

Figure 6. Optical images of 100 μm patterned coatings exposed to 754 J cm^{-2} dose. The dark areas are the patterned phenylsilane coating while the bright regions are the exposed substrate (silicon). All the images refer to the same scale bar.

range. The Raman image confirms that X-rays are decomposing the anthracene only in the exposed region. Figure 7d illustrates that only in the unirradiated area is the integrity of the anthracene molecules preserved; a similar result was found for pentacene. Therefore, DXRL can be used to selectively decompose acene molecules even in a 40 μm thick coating. This result represents a new route to spatially control the presence of acene species, and it opens a new possibility to fabricate thick planar devices which exploit the acene properties.[31]

Figure 8a shows the SEM images of an irradiated and etched C_{60}-doped phenylsilane film and the pattern appears uniform and well-defined. Figure 8b proves that the vertical profile is almost perpendicular to the silicon substrate even in a 40 μm thick doped coating; in fact, the measured TS/BS ratio is about 0.98. To investigate the effect of hard X-rays in such coating, we also used in this case Raman spectroscopy. In particular, the 1500−1420 cm^{-1} region has been monitored before and after the X-ray irradiation process; the spectrum of pure fullerene is reported for reference. The Raman signal of the unexposed doped coating with C_{60} is presented in Figure 8c. The 1467 cm^{-1} signal corresponds to that one detected in the fullerene powder and it is attributed to the C_{60} A_g mode.[32] Surprisingly,

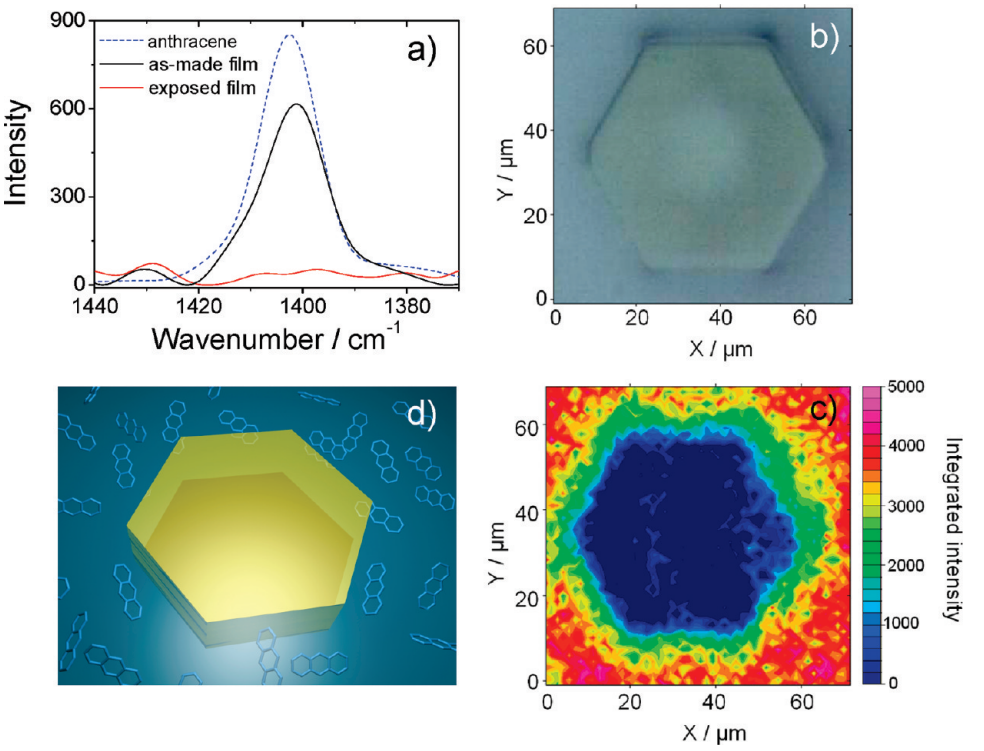

Figure 7. (a) Raman spectra in the 1440−1370 cm^{-1} range of a hybrid phenylsilane film doped with anthracene before and after X-ray exposure (black and red line, respectively). The blue dot line is the spectrum of pure anthracene reported as the reference. (b) Optical images of an irradiated coating before chemical development process; the hexagonal perimeter represents the interface between the irradiated region (inside) and the unirradiated region (outside). (c) Raman mapping in the same area obtained integrating the $6A_g$ mode in the 1420−1380 cm^{-1} range. (d) Illustration of the coating after irradiation. In the exposed regions, the anthracene molecules are selectively decomposed.

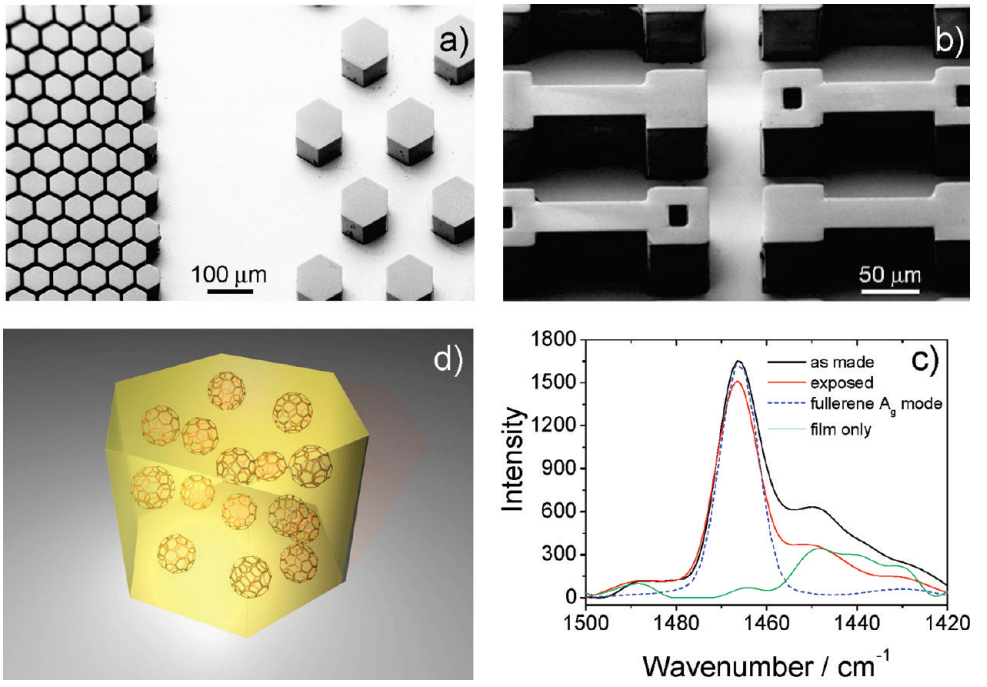

Figure 8. (a, b) SEM images at different magnification of an irradiated and etched C_{60} doped phenylsilane film. The thickness of the coating is around 40 μm. (c) Raman spectra in the 1500−1420 cm^{-1} range of a phenylsilane film doped with fullerene before and after X-ray exposure (black and red line, respectively). The green line and the blue dot line represent the spectra of pure phenylsilane and C_{60} respectively. (c) Illustration of patterned hexagonal pillars containing fullerenes.

the X-ray patterning processes do not appreciably changed the amount of fullerene detected. In fact, just a slight intensity change of such mode is observed. Probably fullerene derivatives are also produced during the X-ray irradiation process by radicalic

reactions between C_{60} and the hybrid silica network. However, fullerene and its derivates do present the same A_g mode at 1467 cm^{-1} [33]. This is enough to ensure that C_{60} is more stable than acenes under X-rays exposure, and that its properties remain unvaried after the overall patterning process. Therefore, DXRL offers a new and fast route to fabricate devices based on hybrid thick patterns for nonlinear or optical limiting applications.

CONCLUSIONS

We have demonstrated the possibility to use hard X-rays to pattern thick coatings based on phenylsilane; high quality patterns can be fabricated without the need of additional resists or chemical modifications. A lithography protocol to achieve patterns up to 100 μm thick has been optimized and high aspect ratio structures have been obtained. The study by FTIR of the effect of the radiation during the DXRL patterning process has revealed that the minimum energy needed to achieve good-quality patterns corresponds to a condensation of around 50% of the initial silanol content. We have demonstrated that such phenylsilane coating can host a variety of polycyclic aromatic hydrocarbon functional molecules such as anthracene, pentacene, and fullerene. Because X-rays decompose anthracene and pentacene molecules in the irradiated regions, DXRL can be used for writing such functionality even in thick coatings. A different result has been found for C_{60}. In fact, X-rays do not appreciably affect the fullerene molecules used to dope the phenylsilane films. The addition of such carbon-based molecules does not affect the microfabrication process, the quality of the lithographed structure or the homogeneity of the final patterned material.

ASSOCIATED CONTENT

Supporting Information. Emission spectra of anthracene-doped sol−gel film, photoluminescence and optical absorption of C60-doped phenylsilane films (PDF). This information is available free of charge via the Internet at http://pubs.acs.org/.

AUTHOR INFORMATION

Corresponding Author

*E-mail: plinio@uniss.it (P.I.); paolo.falcaro@csiro.au (P.F.).

ACKNOWLEDGMENT

We acknowledge travel funding provided by the International Synchrotron Access Program (ISAP) managed by the Australian Synchrotron. The ISAP is an initiative of the Australian Government being conducted as part of the National Collaborative Research Infrastructure Strategy. The CSIRO OCE Science Leader Scheme is acknowledged for supporting this work. DB acknowledges the Australian Research Council (ARC) for the support through the APD Discovery grant DP0988106.

REFERENCES

(1) Falcaro, P.; Malfatti, L.; Vaccari, L.; Amenitsch, H.; Marmiroli, B.; Grenci, G.; Innocenzi, P. *Adv. Mater.* **2009,** *21*, 4932.

(2) Buso, D.; Della Giustina, G.; Brusatin, G.; Guglielmi, M.; Martucci, A.; Chiasera, A.; Ferrari, M.; Romanato, F. *J. Nanosci. Nanotech.* **2009,** *9* (3), 1858.

(3) Falcaro, P.; Innocenzi, P. *J. Sol−Gel Sci. Technol.* **2010**, in press, 10.1007/s10971-009-2127-7.

(4) Innocenzi, P.; Kidchob, T.; Costacurta, S.; Falcaro, P.; Cacho-Nerin, F.; Marmiroli, B.; Amenitsch, H. *Soft Matter.* **2010,** *6*, 3172.

(5) Falcaro, P.; Costacurta, S.; Malfatti, L.; Kidchob, T.; Takahashi, M.; Casula, M.; Piccinini, M.; Marcelli, A.; Marmiroli, B.; Amenitsch, H.; Schiavuta, P.; Innocenzi, P. *Adv. Mater.* **2008,** *20*, 1864.

(6) Falcaro, P.; Malfatti, L.; Kidchob, T.; Giannini, G.; Falqui, A.; Casula, M. F.; Amenitsch, H.; Marmiroli, B.; Grenci, G.; Innocenzi, P. *Chem. Mater.* **2009,** *21*, 2055.

(7) Malfatti, L.; Marongiu, D.; Costacurta, S.; Falcaro, P.; Amenitsch, H.; Marmiroli, B.; Grenci, G.; Casula, M.; Innocenzi, P. *Chem. Mater.* **2010,** *22*, 2132.

(8) Costacurta, S.; Malfatti, L.; Patelli, A.; Amenitsch, H.; Marmiroli, B.; Falcaro, P.; Innocenzi, P. *Plasma Proc. Polym.* **2010,** *7*, 459.

(9) Munnik, F.; Benninger, F.; Mikhailov, S.; Bertsch, A.; Renaud, P.; Lorenz, H.; Gmur, M. *Microelectron. Eng.* **2003,** *67−68*, 96.

(10) Kupka, R. K.; Bouamrane, F.; Cremers, C.; Megtert, S. *App. Surf. Sci.* **2000,** *164*, 97–110.

(11) Awazu, K.; Wang, X.; Fujimaki, M.; Kuriyama, T.; Sai, A.; Ohki, Y.; Imai, H. *J. Vac. Sci. Technol.. B* **2005,** *23*, 934.

(12) Liu, X.; Cui, T.; Sunkam, R. K.; Coane, P. J.; Vasile, M. J.; Geoettert *Sens. Actuators. B* **2003,** *88*, 75.

(13) Liu, Y.; Cui, T.; Coane, P. J.; Vasile, M. J.; Goettert, J. *Microsyst. Technol.* **2003,** *9*, 171.

(14) Hayase, S. *Prog. Polym. Sci.* **2003,** *28*, 359.

(15) Abdelmalek, F.; Chovelon, J. M.; Lacroix, M.; Jaffrezic-Renault, N.; Matejec, V. *Sens. Actuators B* **1999,** *56*, 234.

(16) Kuniyoshi, M.; Takahashi, M.; Tokuda, Y.; Yoko, T. *J. Non-Cryst. Solids* **2007,** *353*, 4162.

(17) Katsis, D.; Geng, Y. H.; Ou, J. J.: Culligan, S. W.; Trajkovska, A.; Chen, S. H.; Rothberg L. J. *Chem. Mater.* **2002**, *14* (3), pp 1332−1339

(18) Wolak, M. A.; Jang, B-B.; Palilis, L. C.; Kafafi, Z. H. *J. Phys. Chem. B* **2004,** *108* (18), 5492.

(19) Mateo-Alonso, A.; Iliopoulos, K.; Couris, S.; Prato, M. *J. Am. Chem. Soc.* **2008,** *130* (5), 1534.

(20) Innocenzi, P.; Brusatin, G. *Chem. Mater.* **2001,** *13*, 3126.

(21) *User's and Reference Guide for the Scanning Probe Image Processor, SPIP*; Image Metrology A/S: Copenhagen, 2001.

(22) Innocenzi, P.; Brusatin, G. *Chem. Mater.* **2001,** *13*, 3126.

(23) Saraev, V. V.; Alsarsur, I. A.; Annenkov, V. V.; Danilovtseva, E. N. *Russ. J. App. Chem.* **2001,** *74*, 1585.

(24) Nagai, H.; Nakata, Y.; Suzuki, M.; Okutani., T. *J. Mater. Sci.* **1998,** *33*, 1897.

(25) Watanabe, A.; Matsuda, M. *Chem. Lett.* **1991,** 1101.

(26) Ou, D. L.; Seddon, A. B. *J. Non-Cryst. Solids* **1997,** *210*, 187.

(27) Innocenzi, P. *J. Non-Cryst. Solids* **2003,** *316*, 309.

(28) (a) Stuart, B. *Infrared Spectroscopy: Fundamentals and Applications*; J. Wiley & Sons: New York, 2004.(b) Abbate, M; Di Liello, V.; Martuscelli, E.; Musto, P.; Ragosta, G.; Scarinzi, G. *Polymer* **1992,** *33*, 2940.

(29) Jas, G. S.; Wan, C.; Kuczera, K.; Johnson, C. K. *J. Phys. Chem.* **1996,** *100*, 11857.

(30) Shinohara, H.; Yamakita, Y; Ohno, K. *J. Molecul. Struct.* **1998,** *442*, 221.

(31) Menaa, B.; Takahashi, M.; Tokuda, Y.; Yoko, T. *J. Sol−Gel. Sci. Technol.* **2006,** *39*, 185.

(32) Lynch, K.; Tanke, C.; Menzel, F.; Brockner, P.; Scharff, P.; Stumpp, E. *J. Phys. Chem.* **1995,** *99*, 7985.

(33) Innocenzi, P.; Falcaro, P.; Schergna, S.; Maggini, M.; Menna, E.; Amenitsch, H.; Soler-Illia, J. A. A.; Grosso, D.; Sanchez, C. *J. Mater. Chem.* **2004,** *14*, 1838.

NOTE ADDED AFTER ASAP PUBLICATION

This paper was published on the Web on January 10, 2011, and the original version had incorrect affiliations for some of the authors. The corrected version was reposted on January 28, 2011.